

FREQUENCY DOMAIN CALCULATIONS OF ACOUSTIC PROPAGATION

David P. Lockard*

NASA Langley Research Center, Hampton, VA 23681-2199, U.S.A.

ABSTRACT

Two complex geometry problems are solved using the linearized Euler equations. The impedance mismatch method¹ is used to impose the solid surfaces without the need to use a body-fitted grid. The problem is solved in the frequency domain to avoid long run times. Although the harmonic assumption eliminates all time dependence, a pseudo-time term is added to allow conventional iterative methods to be employed. A Jameson² type, Runge-Kutta scheme is used to advance the solution in pseudo time. The spatial operator is based on a seven-point, sixth-order finite difference. Constant coefficient, sixth-derivative artificial dissipation is used throughout the domain. A buffer zone technique employing a complex frequency³ to damp all waves near the boundaries is used to minimize reflections. The results show that the method is capable of capturing the salient features of the scattering, but an excessive number of grid points are required to resolve the phenomena in the vicinity of the solid bodies because the wavelength of the acoustics is relatively short compared with the size of the bodies. Smoothly transitioning into the immersed boundary condition alleviates the difficulties, but a fine mesh is still required.

INTRODUCTION

Problems involving complex geometries are commonplace in real world applications. Although considerable advances have been made in unstructured, multiblock, and overset grid methods, many of the algorithms that can take advantage of these capabilities do not have sufficient accuracy for acoustic problems. Even for high-accuracy methods with these capabilities, generating the grid is non-trivial, especially in three-dimensions. For acoustic problems involving only scattering, Chung and Morris¹ introduced an alternative that allows a Cartesian mesh to be used for arbitrarily complex geometries. All that is required to simulate solid surfaces is to change the density in the regions occupied by the bodies. Although very simple to apply, there are some numerical and resolution issues that will be illustrated in the example problems.

Another difficulty in most acoustic problems is the excessive run time required to wash out initial transients and obtain a periodic steady-state. For linearized problems that are truly periodic, the time dependence can be factored out and the equations solved using algorithms used to accelerate solutions to a steady-state.⁴ Unfortunately, there are difficulties in applying standard acceleration algorithms to the resulting complex equations. Furthermore, for problems with broad frequency content, it is likely to be much more efficient to solve the problem in the time domain with a single computation. However, there are some classes of problems where only the behavior of a few important frequencies are needed.

This paper proceeds by describing a numerical method for solving the harmonic form of the linearized Euler equations and an implementation of the impedance mismatch method for simulating solid bodies. Example problems with two and three cylinders and a periodic source are solved to investigate the merits and disadvantages of the approaches. Some conclusions are made on the efficiency of the method as well as possible extensions.

NUMERICAL METHOD

The linearized Euler equations for a constant mean flow can be written in the form

$$\begin{aligned} \frac{\partial \rho}{\partial t} + \frac{\partial(\rho_o u)}{\partial x} + \frac{\partial(\rho_o v)}{\partial y} &= 0, & \frac{\partial p}{\partial t} + \frac{\partial(\gamma P_o u)}{\partial x} + \frac{\partial(\gamma P_o v)}{\partial y} &= S, \\ \frac{\partial u}{\partial t} + \frac{\partial(p/\rho_o)}{\partial x} &= 0, & \frac{\partial v}{\partial t} + \frac{\partial(p/\rho_o)}{\partial y} &= 0. \end{aligned} \quad (1)$$

The subscript *o* represents mean quantities which are assumed constant. The mean speed of sound and density are used

* Aerospace Technologist

as reference quantities. The ratio of specific heats is denoted by γ . The source term is given by

$$S = \exp\left[-\ln(2)\frac{x^2 + y^2}{0.04}\right] \sin(8\pi t) \quad (2)$$

Equations 1 can be placed in the semi-discrete, compact form

$$\frac{\partial \mathbf{Q}}{\partial t} = -[\mathcal{F}(\mathbf{Q}) - \mathcal{D}(\mathbf{Q})]. \quad (3)$$

Here, \mathcal{F} represents the discrete form of all the spatial derivatives and the source term S appearing in equations 1. A seven point, sixth-order operator is used for all spatial derivatives. \mathcal{D} denotes sixth-derivative, constant coefficient, artificial dissipation. If we assume that all variables have a temporal time dependence of the form $\exp(-i\omega t)$, equation 3 becomes

$$-i\omega \mathbf{Q} \exp(-i\omega t) = -[\mathcal{F}(\mathbf{Q}) - \mathcal{D}(\mathbf{Q})] \exp(-i\omega t). \quad (4)$$

Equation 4 can be solved directly, or an iterative technique can be employed. Direct inversion is the most computationally efficient approach, but the memory requirement can be excessive. Research is ongoing into parallel versions of sparse matrix solvers that may make direct inversion feasible for large problems. However, In the current implementation, the equations are solved iteratively by adding a pseudo-time yielding

$$\frac{\partial \mathbf{Q}}{\partial \tau} = -[\mathcal{F}(\mathbf{Q}) - \mathcal{D}(\mathbf{Q}) - i\omega \mathbf{Q}] = -\mathcal{R}(\mathbf{Q}). \quad (5)$$

Equation 5 is advanced using a Jameson² type, five-stage, Runge-Kutta scheme of the form

$$\begin{aligned} \mathbf{Q}^{(0)} &= \mathbf{Q}^n, \\ \mathbf{Q}^{(s)} &= \mathbf{Q}^n - \frac{\alpha_s \Delta t}{1 + \alpha_s \omega \Delta t} [\mathcal{F}(\mathbf{Q}^{(s-1)}) - \mathcal{D}(\mathbf{Q}^{(s-1)}) - i\omega \mathbf{Q}^{(s-1)}], \\ \mathbf{Q}^{n+1} &= \mathbf{Q}^{(s_{max})} \end{aligned} \quad (6)$$

where n is the iteration counter and $s = 1 \dots 5$ indicates the stage. The values of α_s are $[1/4, 1/6, 3/8, 1/2, 1]$. It should be noted that the stability characteristics of the scheme are considerably different in the complex plane, and the coefficients used in the Runge-Kutta scheme have been modified appropriately. To accelerate convergence, local time-stepping and implicit residual smoothing⁵ are employed. Multigrid acceleration is generally less effective with complex equations, and is not appropriate for immersed boundary conditions because the effective location of the boundary varies with the mesh level.

Boundary Conditions

The impedance mismatch method¹ is used to impose solid bodies within the flow. All that is required is to set the mean density and pressure to 1/30 of their normal values when within solid bodies. Although one would normally expect that using a higher density within solid bodies would yield the desired solution, this problem is difficult to solve numerically because spatial derivatives of the acoustic variables must balance the discontinuities in the mean quantities. Instead, one can cast the governing equations in the form of 1 where the mean quantities are within the spatial derivatives producing smooth fluxes across the solid interfaces. The correct reflected wave is produced, but the solutions within solid bodies are fictitious.

The specified problems are symmetric about $y = 0$, so symmetry is applied using a reflection condition. All other boundaries employ a buffer domain technique³ to minimize reflections. The frequency in equation 6 is made complex in the buffer so that waves are damped. The buffer is four wavelengths thick, and the complex component of the frequency varies as $\omega_i = 2\omega_r(1 - \exp(2d^2))/(1 - \exp(2))$ where d varies from unity at the start of the buffer and is zero at the outer boundary.

RESULTS

Scattering from Two Cylinders

Instantaneous pressure contours for the problem with two cylinders is presented in figure 1. In all cases, a uniform, Cartesian grid is used for the calculations. The grid extended 25 cylinder diameters in the x direction and 8 diameters in

the y direction. The reference cylinder at $(-4,0)$ has a diameter of unity, whereas the cylinder at $(4,0)$ has a diameter of 0.5. Because the impedance mismatch condition is used to simulate the solid cylinders, there is still a solution within the cylinders. However, the values are meaningless. The figure illustrates the complex radiation pattern that results because of the interaction of the scattered fields from the two cylinders and the direct radiation from the source. The lack of contours near the maximum y boundary in figure 1 reveals that the buffer zone boundary condition is damping out the waves. The damped region is not observed in the x direction because the plot has been truncated in that direction.

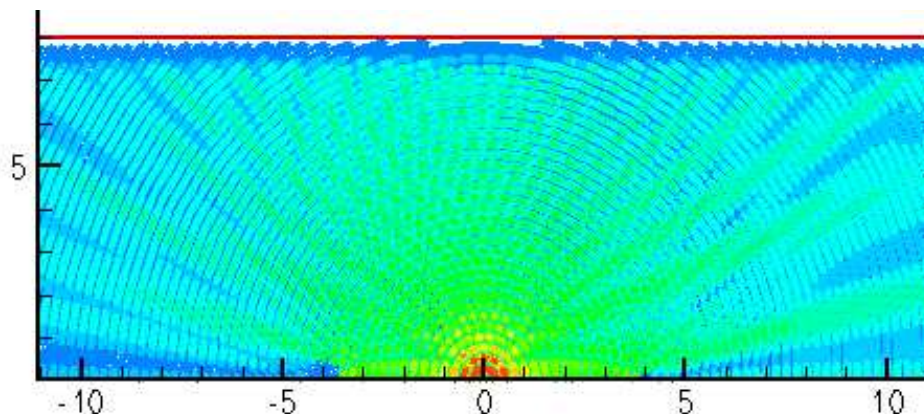


Figure 1: Instantaneous pressure contours for two cylinder problem.

Figure 2 shows averaged p^2 results along the centerline $y = 0$. From figure 2(a), it can be seen that there are some differences between the 15 and 30 points-per-wavelength (PPW) solutions. The PPW are measure along a grid line, so there is less resolution along the diagonal. Figure 2(b) concentrates on the region around the cylinder at $(-4,0)$. The symbols represent the analytic solution. Clearly, neither computational solution is in good agreement with the analytic solution in the vicinity of the cylinder. The amplitude of the oscillations on the side of the cylinder closest to the source ($x > -3.5$) are too low, whereas they appear too high in the shadow region ($x < -4.5$).

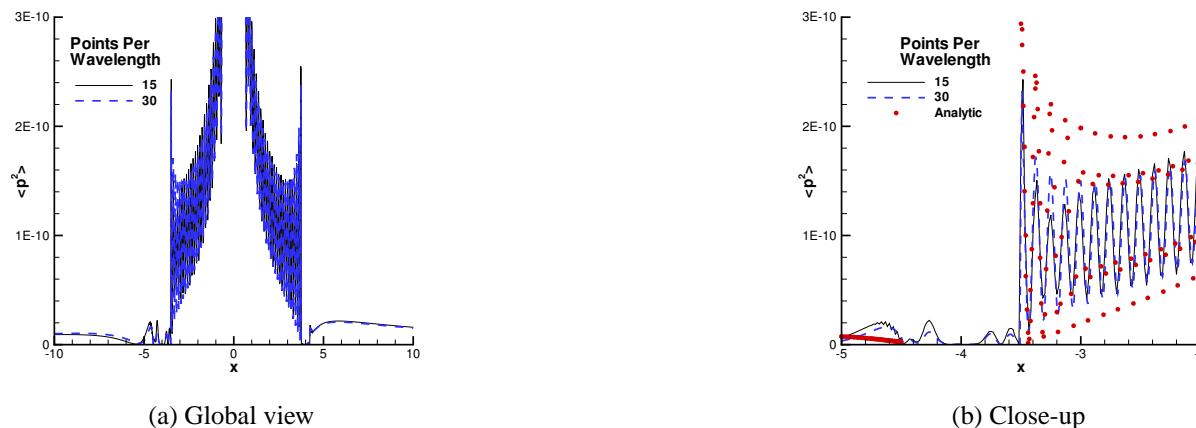


Figure 2: Averaged p^2 results along $y = 0$ for two cylinder problem.

The numerical algorithm can resolve acoustic wave propagation with considerably less than 15 PPW, so the errors are clearly associated with the representation of the cylinders. The actual location of the solid body is somewhat ambiguous with the impedance mismatch method because it occurs between grid lines. Therefore, the boundary changes as the grid is refined. In the current problem, the acoustic wavelength is considerably smaller than the diameter of the cylinders which exacerbates the problem. In addition, although the fluxes are continuous across the interface, the solution variables themselves are not. Hence, there is a difficulty in applying artificial dissipation in this region. This produces numerical oscillations which can contaminate the solution. Furthermore, the solution in the vicinity of the solid bodies is often less accurate than in the far-field. All of these issues contribute to the errors seen in figure 2.

One way to alleviate the numerical errors is to smooth the transition to the lower density within solid bodies. Figure 3(a) compares the density variation in the vicinity of the cylinder using the standard method which abruptly transitions across one grid cell (like a Heaviside function) with that of a $1/2(1 + \cos)$ function that transitions over seven points. The results near the cylinder in figure 3(b) shows that the solution with the smooth transition is in considerably better agreement with the analytic solution than the one employing a Heaviside function transition. However, the method of smoothly varying the density only works well when the distance covered by the transition region is small compared to the acoustic wavelength. Furthermore, it can be difficult to determine in which direction to apply the smooth transition for a general body. Nonetheless, it can produce considerably better results as seen in figure 4 which presents the pressure results on the cylinder surfaces. Because no grid points are actually on the cylinder surfaces, values were interpolated to the surface locations. Considering that the exact location of the surface is ambiguous, the results are reasonably good.

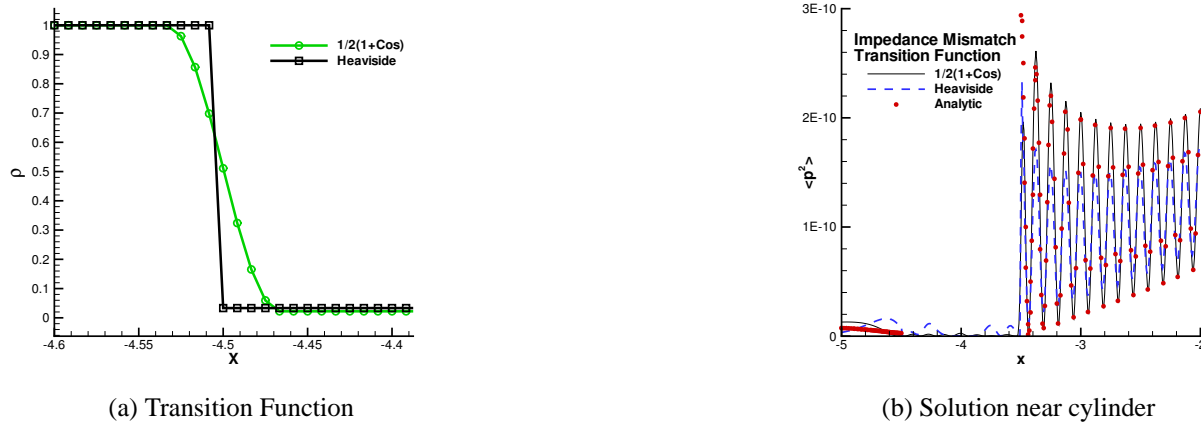


Figure 3: Transition function effect on averaged p^2 results along $y = 0$ for two cylinder problem. The grid has 30 PPW.



Figure 4: Averaged p^2 results on cylinder surfaces for two cylinder problem.

Scattering from Three Cylinders

Instantaneous pressure contours for the problem with three cylinders are presented in figure 5. The grid extended 23 cylinder diameters in the x direction and 12 diameters in the y direction. The reference cylinder at $(-3,0)$ has a diameter of unity, whereas the cylinders at $(3,4)$ and $(3,-4)$ have diameters of 0.75. Considerably more interference is observable compared with the two cylinder solution shown in figure 1.

Figure 6 shows averaged p^2 results along the centerline $y = 0$. Although there are some differences between the solutions with 15 and 30 PPW, they are not as significant as for the two cylinder problem. The close-up view of a solution with a smooth density transition in figure 6(b) does show better agreement with the analytic solution, but it is

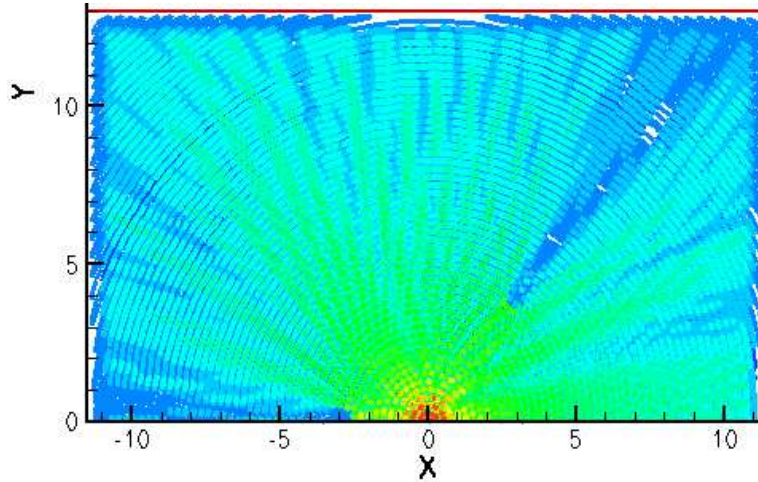


Figure 5: Instantaneous pressure contours for three cylinder problem.

only marginally better than the standard solution with a Heaviside type variation. The orientation and size of the smaller cylinders relative to the larger one may make the effect of secondary reflections less of an issue along the line $y = 0$.

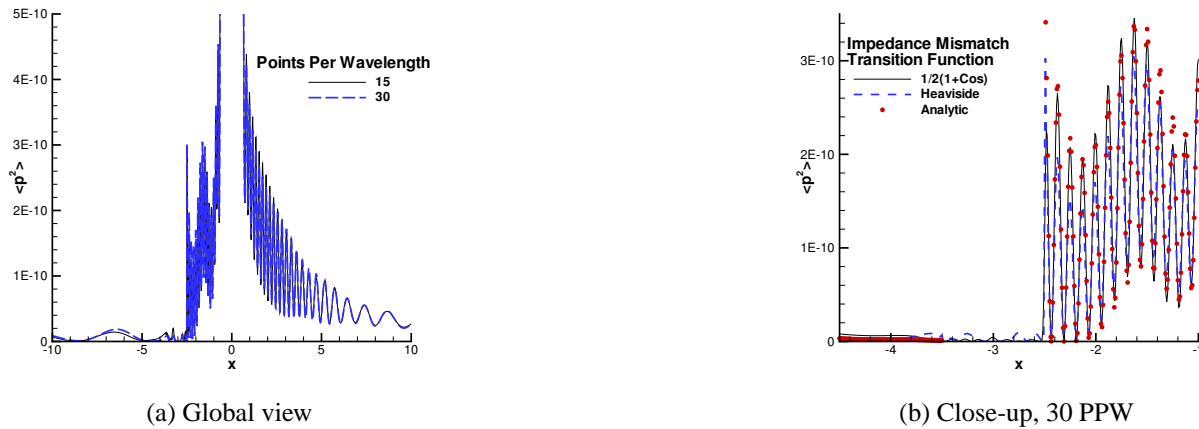


Figure 6: Averaged p^2 results along $y = 0$ for three cylinder problem.

Surface pressure comparisons are presented in figure 7. The solution on the larger cylinder (figure 7(a)) for the case with the smooth density transition does agree better with the analytic solution, but the solution on the smaller cylinder (figure 7(b)) is considerably more wavy than the solution using the standard method. It is unclear why the solution with the smooth density transition exhibits such waviness. Overall, the solutions for the three-cylinder case seem reasonable, although the grids are still excessively fine in order to resolve the regions around the cylinders.

RESOURCES

The CFL number for the calculations was 2.5. Three million grid points and 6241 iterations were used for the two cylinder problem, and 3.8 million points and 6998 iterations for the three-cylinder problem. The residual was forced to drop to $1e-10$ in all cases. However, the solution doesn't vary significantly once the residual drops by several orders of magnitude. Hence, one could decrease the number of iterations by a factor of two and obtain the same basic solution.

A Beowulf cluster of 2.53 GHz Intel Pentium IV computers was used to run the calculations. The two cylinder problem took 16 hours on 36 processors, and the three cylinder problem took 25 hours on the same number of processors. The code used the Message Passing Interface (MPI) to perform communication over a standard Ethernet interconnect. The parallel efficiency is known to be quite low because of a communications bottleneck.

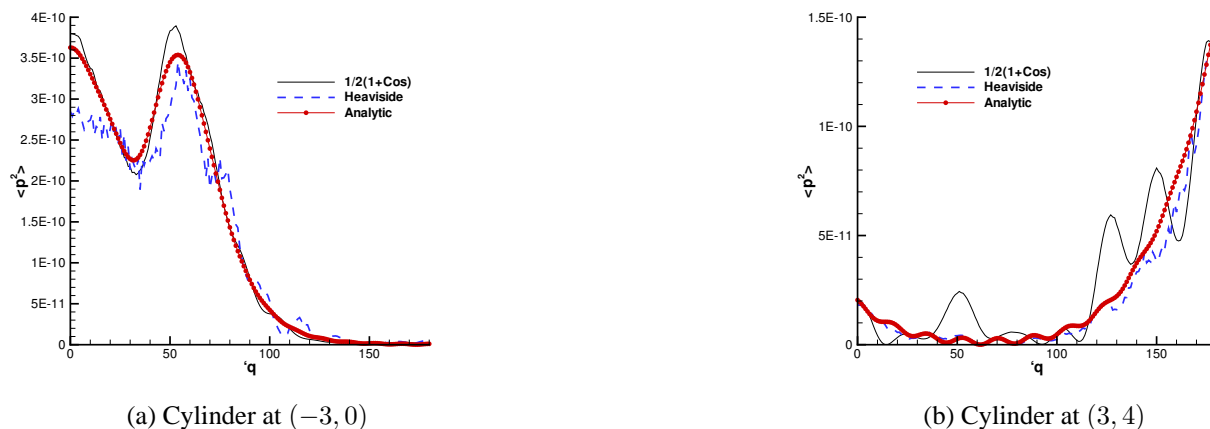


Figure 7: Averaged p^2 results on cylinder surfaces for three cylinder problem. The grid has 30 PPW.

CONCLUSIONS

The performance of the method used in this work is rather disappointing, although the time to generate the grid and make coding changes were almost negligible. The need to have relatively high resolution in the vicinity of solid boundaries necessitated a very fine mesh everywhere because of the aim of using a simple Cartesian grid. The relatively short wavelength of the acoustics relative to the scattering bodies exacerbated the problem. Furthermore, solving the equations in the frequency domain only resulted in a minor improvement in efficiency. Since the grid was uniform, local time stepping was irrelevant. Implicit residual smoothing did allow a slightly larger time step to be used, but the improvement was probably less than a factor of 3. A different iterative technique employing some sort of implicitness may perform better. However, efficient direct solvers with minimal memory requirements hold the most promise. Furthermore, the impedance mismatch method does not appear to be the best choice for problems where detailed information near the scattering bodies is needed. This is especially true for high-frequency phenomena. If only far-field data for lower frequencies is needed, it has already been demonstrated to be useful. However, a finite-element formulation or a multiblock method may prove more useful in general.

REFERENCES

- [1] Chung, C.; and Morris, P. J.: A new boundary treatment for two- and three-dimensional acoustic scattering problems. AIAA-95-008, 1995. Presented at the 1st AIAA/CEAS Aeroacoustics Conference.
- [2] Jameson, A.; Schmidt, W.; and Turkel, E.: Numerical solution of the Euler equations by finite-volume methods using Runge-Kutta time-stepping schemes. AIAA-81-1259, Presented at the 14th AIAA Fluid and Plasma Dynamics Conference, Palo Alto, CA, June 23-25, 1981.
- [3] Agarwal, A.; and Morris, P. J.: The calculation of sound propagation in nonuniform flows: suppression of instability waves. AIAA-03-878, Presented at the 41st AIAA Aerospace Sciences Meeting & Exhibit, Reno, NV, 2003.
- [4] Agarwāl, R. K.; and Huh, K. S.: Acoustic radiation due to gust-airfoil interaction in a compressible flow. CEAS/AIAA Paper-96-1755, 1996. Presented at the 2nd AIAA/CEAS Aeroacoustics Conference, State College, PA, May 6-8.
- [5] Hirsch, C.: *Numerical Computation of Internal and External Flows, Volume 2*. John-Wiley and Sons, 1990.